Orthogonal and antiparallel vortex tubes and energy cascades in quantum turbulence

Tsuyoshi Kadokura and Hiroki Saito
Department of Engineering Science, University of Electro-communications, Tokyo 182-8585, Japan

(Received 7 July 2018; published 17 October 2018)

We investigate the dynamics of energy cascades in quantum turbulence by directly observing the vorticity distributions in numerical simulations of the Gross-Pitaevskii equation. By Fourier filtering each scale of the vorticity distribution, we find that antiparallel vortex tubes at a large scale generate small-scale vortex tubes orthogonal to those at the large scale, which is a manifestation of the energy cascade from large to small scales. We reveal the dynamics of quantized vortex lines in these processes.

DOI: 10.1103/PhysRevFluids.3.104606

I. INTRODUCTION

As the Reynolds number increases, laminar fluid flow develops into turbulence due to hydrodynamic instability [1], and energy is transferred from large to small scales. Such an energy cascade has already been implied in the famous sketch of water turbulence drawn by Leonardo da Vinci, in which many large and small vortices are tangled with each other. More specifically, the energy cascade in turbulence was illustrated by Richardson, in which large-scale vortex rings are divided into small-scale vortex rings [2]. By a statistical approach with universality assumptions, the energy cascade has been shown to lead to Kolmogorov's $-5/3$ power law in the energy spectrum, which has been thoroughly investigated theoretically and observed experimentally [3–12].

Quantum fluids are different from classical fluids in that, in quantum fluids, vortices are quantized and viscosity is absent. Despite these differences, it has been shown that classical and quantum fluids share a variety of hydrodynamic phenomena [13–19]. Energy cascades and power-law spectra have been observed in quantum turbulence of superfluid helium [20] and ultracold atomic gases [21]. Theoretically, it has been revealed that turbulent quantum fluids exhibit Kolmogorov's power law in incompressible kinetic-energy spectra [22–25]. A variety of dynamics and power-law spectra in quantum fluids have been investigated [26–49].

Recently, Goto *et al.* [9,10] numerically studied the energy cascade in classical fluids from the perspective of the vorticity distribution. By taking the Fourier transform of the vorticity distribution and applying a band-pass filter to the Fourier components, they extracted each scale of the vorticity distribution of the turbulent flow. They found that the vortex tubes at each scale tend to align in antiparallel, while vortex tubes generated at smaller scales tend to be orthogonal to the antiparallel vortex tubes at larger scales. This dynamics leads to the energy transfer from large to small scales and may be responsible for the energy cascade and Kolmogorov's power law. Since there are various similarities between the hydrodynamic phenomena in classical and quantum fluids, we expect that the dynamics observed at each hierarchy in the vorticity distribution of classical fluids should also be observed in quantum fluids. We investigate this correspondence in the present study.

In the present paper, we focus on each level of hierarchy in the vorticity distribution in a quantum fluid. First, so that the expected dynamics can be clearly seen, antiparallel vortex bundles are imprinted artificially in a uniform superfluid. Using a method of Fourier filtering, these bundles of quantized vortices are visualized as vortex tubes. We find that antiparallel vortex tubes generate small-scale vortex tubes orthogonal to the antiparallel vortex tubes. Next, we apply our Fourier

filtering scheme to isotropic fully developed turbulence that exhibits Kolmogorov's $-5/3$ power law. By calculating the angles between the directions of the vortex tubes, we confirm the existence of antiparallel correlation at each scale and orthogonal correlations between different scales in the quantum turbulence, as observed for classical turbulence.

This paper is organized as follows. Section II formulates the problem and describes the numerical method. The dynamics of the initially located vortex bundles are studied in Sec. III A. Section III B studies the case of fully developed quantum turbulence. Conclusions are given in Sec. IV.

II. FORMULATION OF THE PROBLEM

We consider the dynamics of a dilute quantum fluid at zero temperature, which is described by the three-dimensional Gross-Pitaevskii equation given by

$$(i-\gamma)\hbar\frac{\partial\Psi}{\partial t}=-\frac{\hbar^2}{2m}\nabla^2\Psi+U(\boldsymbol{r},t)\Psi+g|\Psi|^2\Psi, \tag{1}$$

where $\Psi(\boldsymbol{r},t)$ is the macroscopic wave function, m is the particle mass, $U(\boldsymbol{r},t)$ represents an external potential, and g is the interaction coefficient. The parameter γ in Eq. (1) describes phenomenological dissipation of the energy of the system. The large-wave-number components generated by the energy cascade are predominantly damped, which mimics the thermal dissipation of the energy in classical fluids. If $\gamma=0$, the energy accumulates in the large-wave-number components due to the energy cascade, and Kolmogorov's power law cannot be obtained in fully developed turbulence. We take $\gamma=0.004$ in this study. We normalize the wave function as $\tilde{\psi}=n_0^{-1/2}\Psi$, where n_0 is the particle density $|\Psi|^2$ in a uniform system without U. The length and time are normalized by $\xi=\hbar/(mgn_0)^{1/2}$ and $\tau=\hbar/(gn_0)$, respectively. Equation (1) is then normalized as

$$(i-\gamma)\frac{\partial\tilde{\psi}}{\partial\tilde{t}}=\left[-\frac{1}{2}\tilde{\nabla}^2+\tilde{U}+|\tilde{\psi}|^2\right]\tilde{\psi}, \tag{2}$$

where $\tilde{\nabla}^2=\xi^2\nabla^2$ and $\tilde{U}=U/(gn_0)$.

The flux of the mass current is given by

$$\boldsymbol{J}=\frac{1}{2i}(\tilde{\psi}^\dagger\tilde{\nabla}\tilde{\psi}-\tilde{\psi}\tilde{\nabla}\tilde{\psi}^\dagger)=|\tilde{\psi}|^2\tilde{\nabla}\phi, \tag{3}$$

where ϕ is the phase of $\tilde{\psi}$. The vorticity $\boldsymbol{\Omega}$ is usually defined as the curl of the velocity field, $\boldsymbol{\Omega}=\tilde{\nabla}\times(\boldsymbol{J}/|\tilde{\psi}|^2)=\tilde{\nabla}\times\tilde{\nabla}\phi$. The vorticity $\boldsymbol{\Omega}$ therefore vanishes everywhere except at the singularity of the quantized vortex core. To avoid the singularity in the vorticity distribution, we define the vorticity distribution of the mass current as

$$\boldsymbol{W}=\tilde{\nabla}\times\boldsymbol{J}, \tag{4}$$

which is a smooth function even at the vortex core and numerically tractable. We extract a specific scale of the vorticity distribution by applying the band-pass Fourier filter [10,11],

$$\tilde{\boldsymbol{W}}(\boldsymbol{k},t;k_c)=\begin{cases}\int\boldsymbol{W}(\boldsymbol{r},t)e^{-i\boldsymbol{k}\cdot\boldsymbol{r}}\mathrm{d}\boldsymbol{r} & (k_c/\sqrt{2}<|\boldsymbol{k}|<\sqrt{2}k_c)\\ 0 & (\text{otherwise})\end{cases}, \tag{5}$$

where k_c is the characteristic wave number of the band-pass filter. The band-pass filtered vorticity distribution is thus given by

$$\boldsymbol{W}(\boldsymbol{r},t;k_c)=\frac{1}{V}\sum_{\boldsymbol{k}}\tilde{\boldsymbol{W}}(\boldsymbol{k},t)e^{i\boldsymbol{k}\cdot\boldsymbol{r}}, \tag{6}$$

where $V=L^3$ is the volume of the system. Let us consider vorticity distributions $\boldsymbol{W}(\boldsymbol{r},t;k_c)$ at two scales, $\boldsymbol{W}_1$ and $\boldsymbol{W}_2$, where k_c for $\boldsymbol{W}_2$ is larger than that for $\boldsymbol{W}_1$. We define an angle θ_{12} between

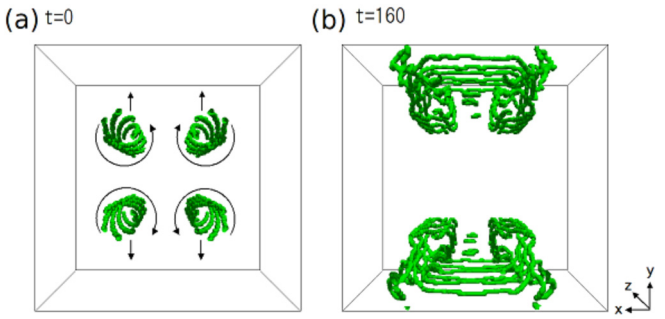

FIG. 1. Dynamics of quantized vortex cores for an initial state with four vortex bundles. The numerical pixels around which the phase rotates by 2π are visualized. (a) Four bundles with six vortex lines in each bundle prepared in a uniform system using Eqs. (9) and (10) with $r_b = 16$. The centers of the bundles are located at $(x, y) = (64, 64), (108, 64), (64, 108)$, and (108,108). The curly arrows indicate the rotation directions of the vortices and the arrows in the $\pm y$ directions indicate the directions of their propagation. (b) Snapshot at $t = 160$. Two pairs of vortex bundles travel in the $\pm y$ directions, and vortex rings and ladder structures are formed. See the Supplemental Material for a movie of the dynamics [51].

$\boldsymbol{W}_1(\boldsymbol{r})$ and $\boldsymbol{W}_2(\boldsymbol{r} + \Delta\boldsymbol{r})$ as

$$\cos\theta_{12} = \frac{\boldsymbol{W}_1(\boldsymbol{r}) \cdot \boldsymbol{W}_2(\boldsymbol{r} + \Delta\boldsymbol{r})}{|\boldsymbol{W}_1(\boldsymbol{r})||\boldsymbol{W}_2(\boldsymbol{r} + \Delta\boldsymbol{r})|}. \tag{7}$$

We also define an angle θ_{11} between $\boldsymbol{W}_1(\boldsymbol{r})$ and $\boldsymbol{W}_1(\boldsymbol{r} + \Delta\boldsymbol{r})$ as

$$\cos\theta_{11} = \frac{\boldsymbol{W}_1(\boldsymbol{r}) \cdot \boldsymbol{W}_1(\boldsymbol{r} + \Delta\boldsymbol{r})}{|\boldsymbol{W}_1(\boldsymbol{r})||\boldsymbol{W}_1(\boldsymbol{r} + \Delta\boldsymbol{r})|}. \tag{8}$$

In numerical calculations, we collect the values of $\cos\theta_{12}$ and $\cos\theta_{11}$ by varying $\boldsymbol{r}$ and $\Delta\boldsymbol{r}$ where $|\Delta\boldsymbol{r}|$ is restricted to some range. We thus obtain the occurrence distributions $P_{12}(\cos\theta_{12})$ and $P_{11}(\cos\theta_{11})$ for these angles. These distributions thus correspond to the probability distributions of the angle between the vorticities, if we choose $\boldsymbol{r}$ (and $\Delta\boldsymbol{r}$ within some range) randomly. If the vorticities $\boldsymbol{W}_1$ at $\boldsymbol{r}$ and $\boldsymbol{r} + \Delta\boldsymbol{r}$ tend to be antiparallel with each other, $P_{11}(\cos\theta_{11})$ has a peak at $\cos\theta_{11} = -1$. If the vorticity $\boldsymbol{W}_1(\boldsymbol{r})$ at a larger scale generates the vorticity $\boldsymbol{W}_2(\boldsymbol{r} + \Delta\boldsymbol{r})$ at a smaller scale and the latter tends to be orthogonal to the former, $P_{12}(\cos\theta_{12})$ has a peak at $\cos\theta_{12} = 0$. These tendencies in $\boldsymbol{W}_1$ and $\boldsymbol{W}_2$ will be numerically shown in the next section.

We numerically solve Eq. (2) using the pseudospectral method, and therefore, a periodic boundary condition is imposed. The numerical space is taken to be $L^3 = 128^3$ with mesh of $\Delta x = \Delta y = \Delta z = 1$.

III. NUMERICAL RESULTS

A. Dynamics of vortex bundles

First we consider the dynamics starting from an artificial initial state to clearly see how large-scale vortex bundles generate vortices at a small scale. Four large-scale vortex bundles are imprinted in a uniform system, as shown in Fig. 1(a) [50]. Each bundle consists of six quantized vortex lines, expressed as

$$\tilde{\psi}(\boldsymbol{r}) = \tilde{\psi}_0(\boldsymbol{r}) \prod_{n=0}^{5} \frac{x - x_n \pm i(y - y_n)}{|x - x_n \pm i(y - y_n)|}, \tag{9}$$

$$\begin{pmatrix} x_n \\ y_n \end{pmatrix} = \begin{pmatrix} r_b \cos\left(\frac{n\pi}{3} \pm \frac{\pi z}{L}\right) \\ r_b \sin\left(\frac{n\pi}{3} \pm \frac{\pi z}{L}\right) \end{pmatrix}, \quad (n = 0, 1, \ldots, 5), \tag{10}$$

where $\tilde{\psi}_0$ is a uniform wave function, r_b is the bundle radius, and the rotation directions of the vortices are determined by the $\pm$ sign in Eq. (9). The time evolution of the system is obtained by solving Eq. (2) with $\tilde{U} = 0$. To extract the vortex cores in Fig. 1, we calculate the phase winding around each numerical mesh. In the time evolution, the two pairs of vortex bundles with opposite circulations first travel in the $\pm y$ directions. Because of the twisted configuration, fast spreading of the vortices in the bundles is avoided. At a later time, small vortex rings are created between the bundles, which are stretched to become ladder-like vortices perpendicular to the bundles, followed by the creation of new vortex rings, as shown in Fig. 1(b).

Figure 2 shows this process in detail. Small vortex rings are nucleated between the vortex bundles, as shown in Fig. 2(b), since the flow velocity in this region exceeds a local critical velocity. We note that such vortex-ring creation is peculiar to the Gross-Pitaevskii model and never occurs in the vortex-filament model [12]. The created vortex rings are then stretched and touch one of the vortices in the bundle, at which vortex reconnection occurs, as shown in Figs. 2(c)–2(e). After the reconnection, the vortices form bridges between the bundles and a ladder structure is formed. Subsequently, new vortex rings are then created between the bundles, as shown in Fig. 2(f). The dynamics of the quantized vortex cores thus clarifies the elementary process of vortex stretching in quantum fluids. The band-pass filtered vorticity distributions $|\boldsymbol{W}_1|$ and $|\boldsymbol{W}_2|$ are shown in Figs. 2(a′)–2(f′). The wave-number ranges of the band-pass filters are $4/\sqrt{2} \leqslant |\boldsymbol{k}| < 4\sqrt{2}$ for $\boldsymbol{W}_1$ and $7/\sqrt{2} \leqslant |\boldsymbol{k}| < 7\sqrt{2}$ for $\boldsymbol{W}_2$; i.e., $\boldsymbol{W}_1$ and $\boldsymbol{W}_2$ are larger and smaller scale vorticity distributions, respectively. At $t = 40$, the vorticities $\boldsymbol{W}_2$ are distributed in and around $\boldsymbol{W}_1$, as shown in Fig. 2(a′). As the vortices in the bundles expand, the distribution $\boldsymbol{W}_1$ diffuses, and the tubelike isodensity surfaces of $\boldsymbol{W}_1$ become thinner. Although the distribution of $\boldsymbol{W}_2$ is fragmented for $t \lesssim 120$, the vortex tubes of $\boldsymbol{W}_2$ that are orthogonal to those of $\boldsymbol{W}_1$ are established at $t = 160$, as shown in Fig. 2(f′). These dynamics clearly show that a large-scale structure produces a small-scale structure, which causes the energy cascade. Similar dynamics are also observed in classical fluids [10,52], which are attributed to vortex stretching. On the other hand, in the present case, the orthogonal structure is generated through stretching of quantized vortex rings and their reconnection [53].

Figures 3(a) and 3(b) show the vortex-core distribution and band-pass filtered vortex distributions of the ladder structure in Figs. 2(f) and 2(f′) seen from different angles. The rotation directions of $\boldsymbol{W}_1$ and $\boldsymbol{W}_2$ are shown in Fig. 3(b), indicating that the adjacent small-scale vortex tubes have opposite rotation directions. To quantify the distributions of the angles between the vortex tubes, we calculate the distributions of $\cos\theta_{12}$ and $\cos\theta_{11}$ for the state in Fig. 3(b), which are shown in Figs. 3(c) and 3(d). The distance $|\Delta\boldsymbol{r}|$ in Eqs. (7) and (8) is taken to be 48–50, which is the typical distance for the distances between vortex tubes in Fig. 3(b). The distribution $P_{12}(\cos\theta_{12})$ is large around $\cos\theta_{12} = 0$, which indicates that $\boldsymbol{W}_1(\boldsymbol{r})$ and $\boldsymbol{W}_2(\boldsymbol{r} + \Delta\boldsymbol{r})$ tend to be orthogonal to each other. The distribution $P_{11}(\cos\theta_{11})$ is large at $\cos\theta_{11} = -1$, which indicates that $\boldsymbol{W}_1(\boldsymbol{r})$ and $\boldsymbol{W}_1(\boldsymbol{r} + \Delta\boldsymbol{r})$ tend to be antiparallel with each other. The peak at $\cos\theta_{11} = 1$ is trivial: the case in which $\boldsymbol{W}_1(\boldsymbol{r})$ and $\boldsymbol{W}_1(\boldsymbol{r} + \Delta\boldsymbol{r})$ are in the same vortex tube. These results are similar to those in classical fluids with a similar setup [10].

B. Fully developed isotropic turbulence

We next consider the case of isotropic quantum turbulence generated by a time-dependent random potential, in which the artificially distributed vortex bundles in Sec. III A are not used and the initial state is the homogeneous state. We numerically solve Eq. (2) with a time-dependent random potential $U(\boldsymbol{r}, t)$ generated by the method given in Appendix A. The system evolves until the steady turbulent state is reached. The isodensity surfaces of $|\tilde{\psi}|^2$, the vortex-core profiles, and the power spectra $E(k)$ are shown in Figs. 4(a)–4(c), 4(a′)–4(c′), and 4(a″)–4(c″), respectively. The power spectrum $E(k)$ is defined in Appendix B. Since the characteristic spatial scale of the random potential is of the order of the system size, long-wavelength modes are excited at $t = 20$. An energy cascade from the long-wavelength to short-wavelength modes then occurs. Kolmogorov's power

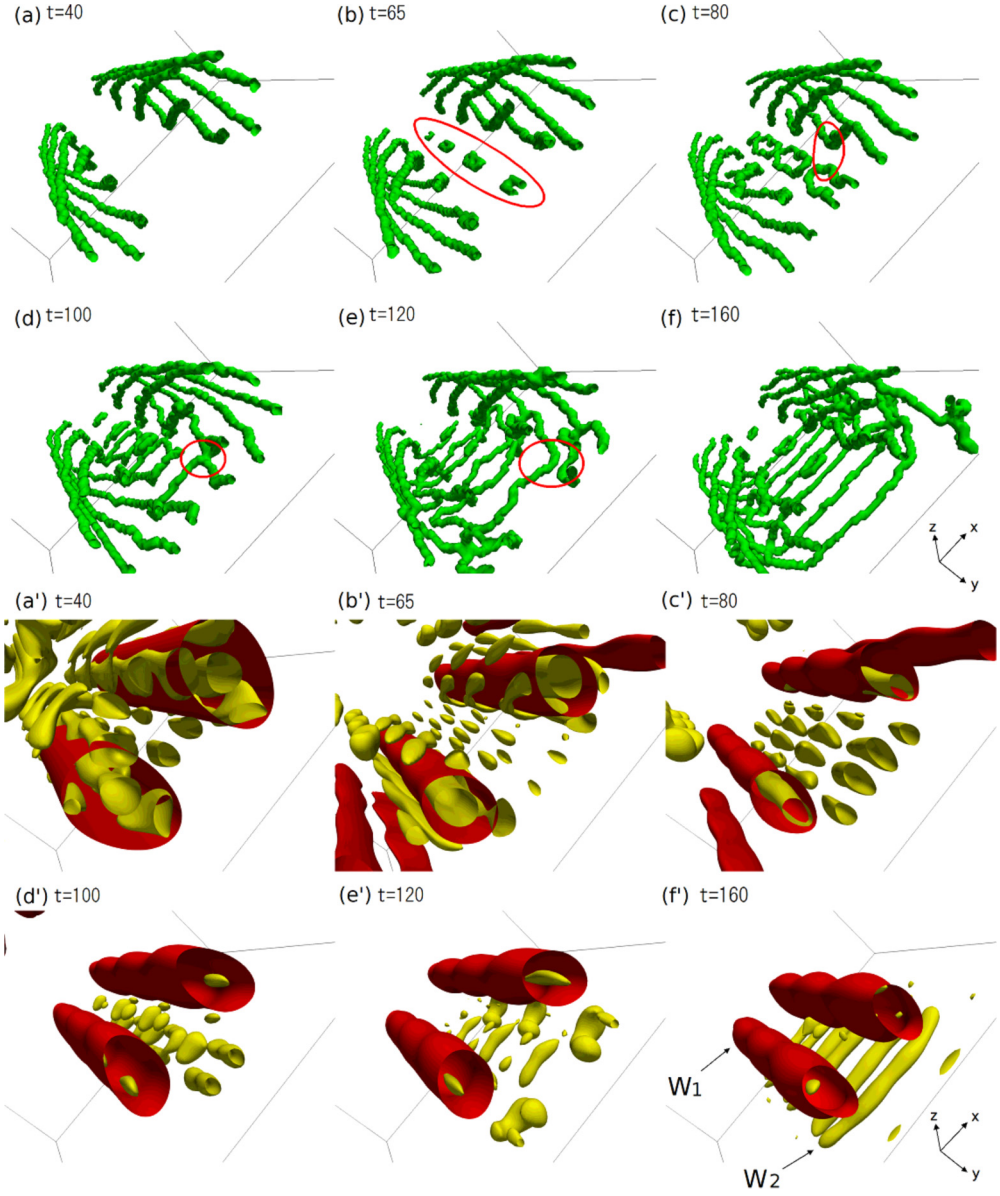

FIG. 2. The same dynamics as in Fig. 1. The vortex cores are shown in panels (a)–(f), and the isodensity surfaces of band-pass filtered vorticity distributions $|\boldsymbol{W}_1|$ and $|\boldsymbol{W}_2|$ are shown in panels (a′)–(f′). The ranges of the wave numbers in the Fourier filters are $4/\sqrt{2} \leqslant |\boldsymbol{k}| < 4\sqrt{2}$ for $\boldsymbol{W}_1$ (red or dark gray) and $7/\sqrt{2} \leqslant |\boldsymbol{k}| < 7\sqrt{2}$ for $\boldsymbol{W}_2$ (yellow or light gray). The outline in panel (b) indicates the created vortex rings. The outlines in panels (c)–(e) highlight vortex reconnection. See the Supplemental Material for movies of the dynamics [51].

law, $E(k) \propto k^{-5/3}$, first appears in the small region of k, as shown in Fig. 4(b″), which grows in time, and the power spectrum reaches a steady profile for $t \gtrsim 2000$, as shown in Fig. 4(c″).

To investigate how the energy is transferred from large to small scales, we calculate the band-pass filtered vorticity distributions $\boldsymbol{W}_1$ and $\boldsymbol{W}_2$. Figure 5(a) shows the isodensity surfaces of $|\boldsymbol{W}_1|$ and $|\boldsymbol{W}_2|$ at $t = 13\,405$. The definitions of $\boldsymbol{W}_1$ and $\boldsymbol{W}_2$ are the same as those in Sec. III A; i.e., $\boldsymbol{W}_1$

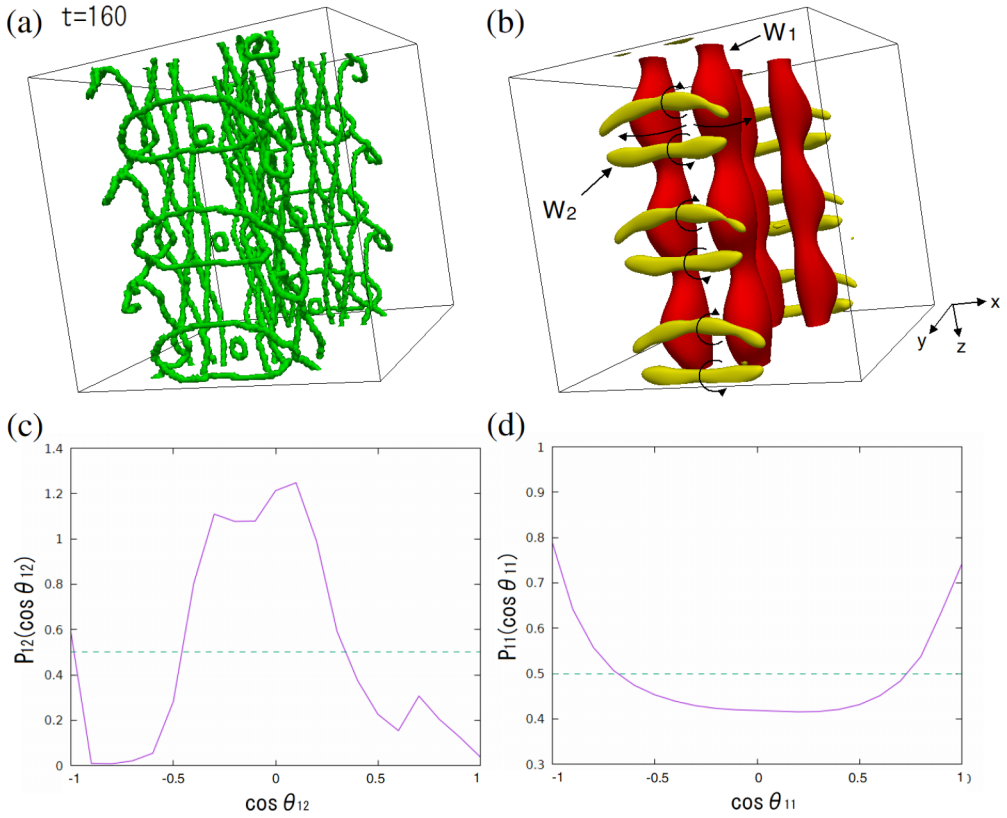

FIG. 3. (a) Vortex cores, (b) isodensity surfaces of $|\boldsymbol{W}_1|$ and $|\boldsymbol{W}_2|$, (c) normalized distribution of angles θ_{12} between $\boldsymbol{W}_1(\boldsymbol{r})$ and $\boldsymbol{W}_2(\boldsymbol{r}+\Delta\boldsymbol{r})$, and (d) normalized distribution of angles θ_{11} between $\boldsymbol{W}_1(\boldsymbol{r})$ and $\boldsymbol{W}_1(\boldsymbol{r}+\Delta\boldsymbol{r})$ at $t = 160$ in the dynamics shown in Fig. 2. The curly arrows in panel (b) represent the directions of the circulations. In panels (c) and (d), the data are taken for the range $48 \leqslant |\Delta\boldsymbol{r}| < 50$. The dashed lines in panels (c) and (d) indicate P_{12} and P_{11} in the case that θ_{12} and θ_{11} would distribute randomly.

and $\boldsymbol{W}_2$ correspond to larger and smaller scale vorticity distributions, respectively. The right-hand panel in Fig. 5(a) shows an enlarged view of the meshed region. In the enlarged view, we can clearly see that the pair of vortex tubes in $\boldsymbol{W}_1$ aligns in parallel and the vortex tubes in $\boldsymbol{W}_2$ tend to be orthogonal to those in $\boldsymbol{W}_1$. This configuration of vortex tubes in $\boldsymbol{W}_1$ and $\boldsymbol{W}_2$ is similar to that in Fig. 3(b) in which the vortex bundles are artificially generated. By contrast, we note that the structures shown in Fig. 5(a) are formed by a random potential. Figures 5(b) and 5(c) show the angular distributions P_{12} and P_{11} of the vorticities $\boldsymbol{W}_1$ and $\boldsymbol{W}_2$, defined in Eqs. (7) and (8). These were calculated for the whole $L^3 = 128^3$ region. Although the turbulent state is induced by a random potential, there are significant correlations between the vorticities. The vorticities $\boldsymbol{W}_1(\boldsymbol{r})$ and $\boldsymbol{W}_2(\boldsymbol{r}+\Delta\boldsymbol{r})$ tend to be orthogonal to each other, and $P_{12}(\cos\theta_{12})$ has a peak at $\cos\theta_{12} = 0$. The vorticities $\boldsymbol{W}_1$ at $\boldsymbol{r}$ and $\boldsymbol{r}+\Delta\boldsymbol{r}$ tend to be antiparallel with each other, and $P_{11}(\cos\theta_{11})$ has a peak at $\cos\theta_{11} = -1$. (The peak at $\cos\theta_{11} = 1$ is due to the correlation within a single vortex tube.) To assure that these tendencies are not incidental, we calculate the time-averaged angular distributions for $13\,000 \leqslant t < 14\,000$. The characteristic timescale of the random potential is $\kappa^{-1} = 20$, which is long enough to observe the ensemble averaged behaviors. We find that the tendencies in Figs. 5(d) and 5(e) are the same as those in Figs. 5(b) and 5(c), respectively, and therefore the above angular correlations in the vorticity distributions can be observed constantly.

Thus, we have shown that in quantum turbulence, large-scale vorticity $\boldsymbol{W}_1$ tends to have antiparallel structures and small-scale vorticity $\boldsymbol{W}_2$ tends to be perpendicular to $\boldsymbol{W}_1$. These results indicate

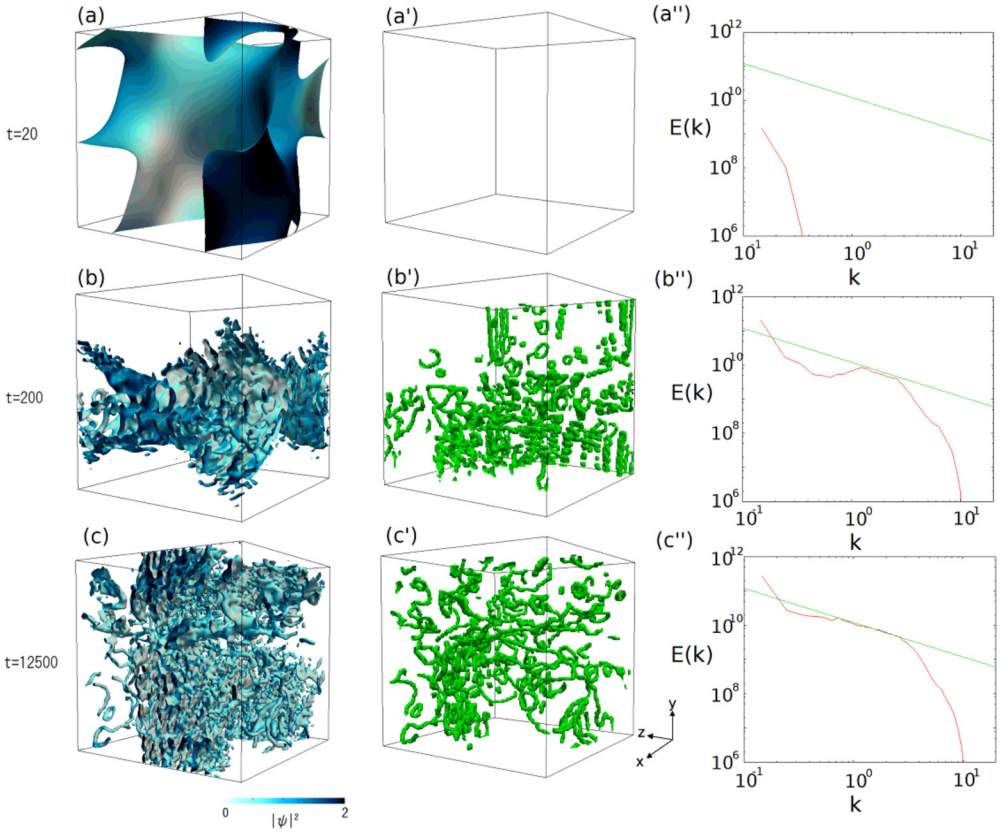

FIG. 4. [(a)–(c)] Isodensity surfaces of $|\tilde{\psi}|^2$, [(a′)–(c′)] vortex-core profiles, and [(a″)–(c″)] power spectra $E(k)$ (arbitrary units) for the dynamics driven by the random potential $U(\boldsymbol{r}, t)$ in Eq. (A1) with $\kappa = 0.05$, $A_0 = 0.5$, and $l = 8\pi$. The size of the cubes in panels (a)–(c) and (a′)–(c′) is 128^3. The slope of the lines in panels (a″)–(c″) is $-5/3$. See the Supplemental Material for a movie of the dynamics in panels (a′)–(c′) [51].

that the energy is transferred from large to small scales through vortex stretch dynamics, which implies that this is one of the mechanisms of the energy cascade and emergence of Kolmogorov's law in quantum turbulence, in addition to the simple vortex reconnection dynamics [26,48].

IV. CONCLUSIONS

We have investigated the dynamics of vortices in quantum fluids using the numerical simulation of the Gross-Pitaevskii equation. We defined band-pass-filtered vorticity distributions to study the dynamics at each scale. In Sec. III A, we examined the dynamics of the vortex bundles and observed that large-scale antiparallel vortices nucleate small-scale vortices orthogonal to those at the large scale. These processes are induced by nucleation of quantized vortex rings and their reconnections. In Sec. III B, we applied our method to the homogeneous isotropic turbulent state. Despite the fact that the turbulent state is generated by a random potential, there are significant correlations in the vorticity distributions. We found that intrascale vorticities tend to align in antiparallel and the smaller scale vortices tend to be orthogonal to larger scale vortices. These vortex dynamics may play an important role in the energy cascade and Kolmogorov's law in quantum turbulence.

In the present study, we have only considered vorticity distributions at two scales $\boldsymbol{W}_1$ and $\boldsymbol{W}_2$. Performing numerical simulations in a larger system will provide vorticity distributions at multiple scales, which will reveal the multistage generation of antiparallel and orthogonal vortices.

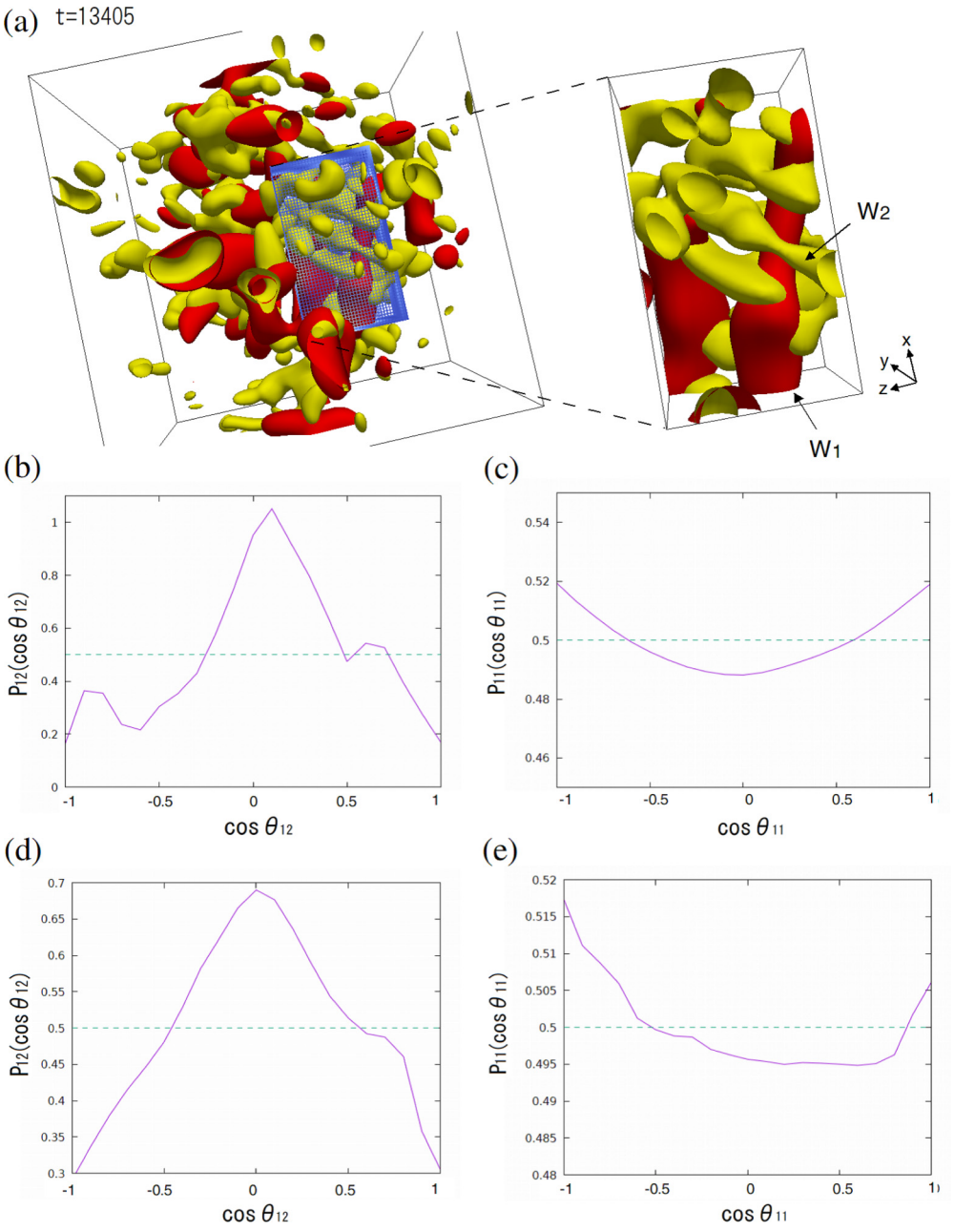

FIG. 5. Vorticity distribution of fully developed turbulence for the dynamics shown in Fig. 4. (a) Isodensity surfaces of vorticity distributions $|\boldsymbol{W}_1|$ and $|\boldsymbol{W}_2|$ at $t = 13405$, where the wave-number ranges of the Fourier filtering are the same as those in Fig. 2. The magnified region clearly shows that $\boldsymbol{W}_1$ and $\boldsymbol{W}_2$ tend to be orthogonal to each other. (b) Distribution of angles θ_{12} between $\boldsymbol{W}_1(\boldsymbol{r})$ and $\boldsymbol{W}_2(\boldsymbol{r} + \Delta\boldsymbol{r})$. (c) Distribution of angles θ_{11} between $\boldsymbol{W}_1(\boldsymbol{r})$ and $\boldsymbol{W}_1(\boldsymbol{r} + \Delta\boldsymbol{r})$. Panels (b) and (c) were obtained by a single shot at $t = 13405$ and panels (d) and (e) are averages of 1000 shots for $13\,000 \leqslant t < 14\,000$. The dashed lines [(b)–(e)] indicate P_{12} and P_{11} in the case that θ_{12} and θ_{11} would distribute randomly. The distributions P_{11} and P_{12} are calculated over the whole 128^3 region [not restricted to the selected region as in the right panel in panel (a)]. See the Supplemental Material for the dynamics and rotating view of panel (a) [51].

ACKNOWLEDGMENT

The present study was supported by JSPS KAKENHI Grants No. JP16K05505, No. JP17K05595, and No. JP17K05596.

APPENDIX A: TIME-DEPENDENT RANDOM POTENTIAL TO GENERATE QUANTUM TURBULENCE

To generate homogeneous isotropic quantum turbulence, we use a random potential. The potential is expanded as

$$U(\boldsymbol{r},t)=\sum_{\boldsymbol{k}} C_{\boldsymbol{k}}(t)e^{i\boldsymbol{k}\cdot\boldsymbol{r}}. \tag{A1}$$

The time-dependent Fourier components $C_k(t)$ follow the Langevin equation

$$\frac{dC_{\boldsymbol{k}}(t)}{dt}=-\kappa C_{\boldsymbol{k}}(t)+f_{\boldsymbol{k}}(t), \tag{A2}$$

where the constant $\kappa>0$ determines the timescale of potential variation and $f_{\boldsymbol{k}}(t)$ is the Gaussian noise with an average,

$$\langle f_{\boldsymbol{k}}(t)\rangle=0, \tag{A3}$$

and correlation function,

$$\langle f_{\boldsymbol{k}}(t)f_{\boldsymbol{k}'}(t')\rangle=A_{\boldsymbol{k}}\delta_{\boldsymbol{k}\boldsymbol{k}'}\delta(t-t'). \tag{A4}$$

The magnitude $A_{\boldsymbol{k}}$ is given by

$$A_{\boldsymbol{k}}=A_0 e^{-(\frac{l}{2}|\boldsymbol{k}|)^2}, \tag{A5}$$

where the parameter l determines the characteristic scale of the random potential. Using the solution of the Langevin equation in Eq. (A1), we have

$$\langle C_{\boldsymbol{k}}(t)C_{\boldsymbol{k}'}(t')\rangle=\frac{A_{\boldsymbol{k}}}{2\kappa}\delta_{\boldsymbol{k}\boldsymbol{k}'}e^{-\kappa|t-t'|}, \tag{A6}$$

which gives

$$\langle U(\boldsymbol{r},t)U(\boldsymbol{r}',t')\rangle\propto e^{-\kappa|t-t'|}e^{|\boldsymbol{r}-\boldsymbol{r}'|^2/l^2}. \tag{A7}$$

In the numerical simulation in Sec. III B, the coefficients $C_{\boldsymbol{k}}(t)$ numerically evolve according to Eq. (A2). The inverse Fourier transform in Eq. (A1) thus gives the time-dependent random potential with spatial and temporal scales of l and κ^{-1}, respectively.

APPENDIX B: INCOMPRESSIBLE KINETIC-ENERGY POWER SPECTRUM

The kinetic energy of a quantum fluid is expressed as

$$E_{\rm kinetic}=-\frac{1}{2}\int d\boldsymbol{r}\tilde{\psi}^*\tilde{\nabla}^2\tilde{\psi}, \tag{B1}$$

$$=\frac{1}{2}\int d\boldsymbol{r}|\tilde{\nabla}\tilde{\psi}|^2. \tag{B2}$$

Using the transformation, $\tilde{\psi}(\boldsymbol{r})=\sqrt{\rho(\boldsymbol{r})}e^{i\phi(\boldsymbol{r})}$, the kinetic energy can be divided into two terms as

$$E_{\rm kinetic}=\frac{1}{2}\int d\boldsymbol{r}[\rho(\tilde{\nabla}\phi)^2+(\tilde{\nabla}\sqrt{\rho})^2], \tag{B3}$$

$$=E_1+E_2, \tag{B4}$$

where $E_1 = \frac{1}{2}\int d\boldsymbol{r}\rho(\tilde{\nabla}\phi)^2$ corresponds to the classical kinetic energy and $E_2 = \frac{1}{2}\int d\boldsymbol{r}(\tilde{\nabla}\sqrt{\rho})^2$ comes from the quantum pressure. We define $\boldsymbol{w}(\boldsymbol{r}) = \sqrt{\rho(\boldsymbol{r})}\tilde{\nabla}\tilde{\phi}(\boldsymbol{r})$ and its Fourier transform,

$$\tilde{\boldsymbol{w}}(\boldsymbol{k}) = \int \boldsymbol{w}(\boldsymbol{r})e^{-i\boldsymbol{k}\boldsymbol{r}}d\boldsymbol{r}. \tag{B5}$$

The field $\boldsymbol{w}$ is divided into compressible and incompressible parts as

$$\tilde{\boldsymbol{w}}(\boldsymbol{k}) = \frac{\boldsymbol{k}\cdot\tilde{\boldsymbol{w}}(\boldsymbol{k})}{k^2}\boldsymbol{k} + \frac{(\boldsymbol{k}\times\tilde{\boldsymbol{w}})\times\boldsymbol{k}}{k^2}, \tag{B6}$$

$$\tilde{\boldsymbol{w}}_{\mathrm{L}} = \frac{\boldsymbol{k}\cdot\tilde{\boldsymbol{w}}(\boldsymbol{k})}{k^2}\boldsymbol{k}, \tag{B7}$$

$$\tilde{\boldsymbol{w}}_{\mathrm{T}} = \frac{(\boldsymbol{k}\times\tilde{\boldsymbol{w}})\times\boldsymbol{k}}{k^2}. \tag{B8}$$

The kinetic energy can be rewritten as

$$E_1 = \frac{1}{2}\int d\boldsymbol{r}|\boldsymbol{w}(\boldsymbol{r})|^2, \tag{B9}$$

$$= \frac{1}{2}\int d\boldsymbol{r}[|\boldsymbol{w}_{\mathrm{T}}(\boldsymbol{r})|^2 + |\boldsymbol{w}_{\mathrm{L}}(\boldsymbol{r})|^2]. \tag{B10}$$

We focus on the incompressible part of the kinetic energy,

$$E_1^{\mathrm{ic}} = \frac{1}{2}\int |\boldsymbol{w}_{\mathrm{T}}(\boldsymbol{r})|^2 d\boldsymbol{r}, \tag{B11}$$

$$= \frac{1}{2}\int \frac{d\boldsymbol{k}}{(2\pi)^3}\tilde{\boldsymbol{w}}_{\mathrm{T}}(\boldsymbol{k})\cdot\tilde{\boldsymbol{w}}_{\mathrm{T}}(-\boldsymbol{k}), \tag{B12}$$

$$= \int dkE(k), \tag{B13}$$

which is the definition of the power spectrum $E(k)$ of the incompressible flow.

[1] O. Reynolds, An experimental investigation of the circumstances which determine whether the motion of water shall be direct or sinuous and of the law of resistance in parallel channels, Philos. Trans. R. Soc. London **174**, 935 (1883).

[2] L. F. Richardson, *Weather Prediction by Numerical Process* (Cambridge University Press, Cambridge, UK, 1922).

[3] U. Frisch, *Turbulence: The Legacy of A. N. Kolmogorov* (Cambridge University Press, Cambridge, UK, 1995).

[4] A. N. Kolmogorov, The local structure of turbulence in incompressible viscous fluid for very large Reynolds numbers, Dokl. Akad. Nauk SSSR **30**, 299 (1941).

[5] G. K. Batchelor and I. Proudman, The effect of rapid distortion of a fluid in turbulent motion, Q. J. Mech. Appl. Math. **7**, 83 (1954).

[6] T. Tatsumi, The theory of decay process of incompressible isotropic turbulence, Proc. R. Soc. London, Ser. A **239**, 16 (1957).

[7] R. H. Kraichnan, On Kolmogorov's inertial-range theories, J. Fluid Mech. **62**, 305 (1974).

[8] U. Frisch, P. L. Sulem, and M. Nelkin, A simple dynamical model of intermittent fully developed turbulence, J. Fluid Mech. **87**, 719 (1978).

[9] S. Goto, A physical mechanism of the energy cascade in homogeneous isotropic turbulence, J. Fluid Mech. **605**, 355 (2008).
[10] S. Goto, Y. Saito, and G. Kawahara, Hierarchy of antiparallel vortex tubes in spatially periodic turbulence at high Reynolds numbers, Phys. Rev. Fluids **2**, 064603 (2017).
[11] S. Goto, Coherent structures and energy cascade in homogeneous turbulence, Prog. Theor. Phys. Suppl. **195**, 139 (2012).
[12] In the vortex-filament model, vortex rings can be created by the collapse of antiparallel segments of two vortex lines. See, e.g., A. Pumir and E. D. Siggia, Vortex dynamics and the existence of solutions to the Navier-Stokes equations, Phys. Fluids **30**, 1606 (1987); M. Kursa, K. Bajer, and T. Lipniacki, Cascade of vortex loops initiated by a single reconnection of quantum vortices, Phys. Rev. B **83**, 014515 (2011).
[13] K. Sasaki, N. Suzuki, and H. Saito, Bénard–Von Kármán Vortex Street in a Bose-Einstein Condensate, Phys. Rev. Lett. **104**, 150404 (2010).
[14] M. T. Reeves, T. P. Billam, B. P. Anderson, and A. S. Bradley, Identifying a Superfluid Reynolds Number Via Dynamical Similarity, Phys. Rev. Lett. **114**, 155302 (2015)
[15] W. J. Kwon, J. H. Kim, S. W. Seo, and Y. Shin, Observation of Von Kármán Vortex Street in an Atomic Superfluid Gas, Phys. Rev. Lett. **117**, 245301 (2016).
[16] K. Sasaki, N. Suzuki, D. Akamatsu, and H. Saito, Rayleigh-Taylor instability and mushroom-pattren formation in a two-component Bose-Einstein condensate, Phys. Rev. A **80**, 063611 (2009).
[17] T. Kadokura, T. Aioi, K. Sasaki, T. Kishimoto, and H. Saito, Rayleigh-Talor instability in a two-component Bose-Einstein condensate with rotational symmetry, Phys. Rev. A **85**, 013602 (2012).
[18] H. Takeuchi, N. Suzuki, K. Kasamatsu, H. Saito, and M. Tsubota, Quantum Kelvin-Helmholtz instability in phase-separated two-component Bose-Einstein condensates, Phys. Rev. B **81**, 094517 (2010).
[19] A. Bezett, V. Bychkov, E. Lundh, D. Kobyakov, and M. Marklund, Magnetic Richtmyer-Meshkov instability in a two-component Bose-Einstein condensate, Phys. Rev. A **82**, 043608 (2010).
[20] L. Skrbek, Quantum turbulence, J. Phys. Conf. **318**, 012004 (2011).
[21] N. Navon, A. I. Gaunt, R. P. Smith, and Z. Hadzibabic, Emergence of a turbulent cascade in a quantum gas, Nature (London) **539**, 3 (2016).
[22] T. Araki, M. Tsubota, and S. K. Nemirovskii, Energy Spectrum of Superfluid Turbulence with no Normal-Fluid Component, Phys. Rev. Lett. **89**, 145301 (2002).
[23] M. Kobayashi and M. Tsubota, Kolmogorov Spectrum of Superfluid Turbulence: Numerical Analysis of the Gross-Pitaevskii Equation with a Small-Scale Dissipation, Phys. Rev. Lett. **94**, 065302 (2005).
[24] M. Kobayashi and M. Tsubota, Thermal Dissipation in Quantum Turbulence, Phys. Rev. Lett. **97**, 145301 (2006).
[25] M. Kobayashi and M. Tsubota, Quantum Turbulence in a Trapped Bose-Einstein Condensate, Phys. Rev. A **76**, 045603 (2007).
[26] R. M. Kerr and F. Hussain, Simulation of vortex reconnection, Phys. D (Amsterdam, Neth.) **37**, 474 (1989).
[27] M. Tsubota, Quantum turbulence: From superfluid helium to atomic Bose-Einstein condensates, Contemp. Phys. **50**, 463 (2009).
[28] R. M. Kerr, Swirling, turbulent vortex rings formed from a chain reaction of reconnection events, Phys. Fluids **25**, 065101 (2013).
[29] S. K. Nemirovskii, Quantum turbulence: Theoretical and numerical problems, Phys. Rep. **524**, 85 (2013).
[30] G. V. Kolmakov, P. V. E. McClintok, and S. V. Nazarenko, Wave turbulence in quantum fluids, Proc. Natl. Acad. Sci. USA **111**, 4727 (2014).
[31] C. F. Barenghi, L. Skrbek, and K. R. Sreenivasan, Introduction to quantum turbulence, Proc. Natl. Acad. Sci. USA **111**, 4647 (2014).
[32] P. Walmsley, D. Zmeev, F. Pakpour, and A. Golov, Dynamics of quantum turbulence of different spectra, Proc. Natl. Acad. Sci. USA **111**, 4691 (2014).
[33] R. Hänninen and A. W. Baggaley, Vortex filament method as a tool for computational visualization of quantum turbulence, Proc. Natl. Acad. Sci. USA **111**, 4667 (2014).
[34] A. C. White, B. P. Anderson, and V. S. Bagnato, Vortices and turbulence in trapped atomic condensates, Proc. Natl. Acad. Sci. USA **111**, 4719 (2014).

[35] C. F. Barenghi, V. S. L'vov, and P. E. Roche, Experimental, numerical, and analytical velocity spectra in turbulent quantum fluid, Proc. Natl. Acad. Sci. USA **111**, 4683 (2014).
[36] M. Tsubota, K. Fujimoto, and S. Yui, Numerical studies of quantum turbulence, J. Low Temp. Phys. **188**, 119 (2017).
[37] M. Tsubota and M. Kobayashi, Quantum turbulence in trapped atomic Bose-Einstein condensates, J. Low Temp. Phys. **150**, 402 (2008).
[38] C. Nore, M. Abid, and M. E. Brachet, Kolmogorov Turbulence in Low-Temperature Superflows, Phys. Rev. Lett. **78**, 3896 (1997).
[39] J. Paret and P. Tabeling, Experimental Observation of the Two-Dimensional Inverse Energy Cascade, Phys. Rev. Lett. **79**, 4162 (1997).
[40] S. R. Stalp, L. Skrbek, and R. J. Donnelly, Decay of Grid Turbulence in a Finite Channel, Phys. Rev. Lett. **82**, 4831 (1999).
[41] K. W. Madison, F. Chevy, W. Wohlleben, and J. Dalibard, Vortex Formation in a Stirred Bose-Einstein Condensate, Phys. Rev. Lett. **84**, 806 (2000).
[42] D. Kivotides, J. C. Vassilicos, D. C. Samuels, and C. F. Barenghi, Kelvin Waves Cascade in Superfluid Turbulence, Phys. Rev. Lett. **86**, 3080 (2001).
[43] N. G. Parker and C. S. Adams, Emergence and Decay of Turbulence in Stirred Atomic Bose-Einstein Condensates, Phys. Rev. Lett. **95**, 145301 (2005).
[44] P. M. Walmsley, A. I. Golov, H. E. Hall, A. A. Levchenko, and W. F. Vinen, Dissipation of Quantum Turbulence in the Zero Temperature Limit, Phys. Rev. Lett. **99**, 265302 (2007).
[45] A. W. Baggaley, J. Laurie, and C. F. Barenghi, Vortex-Density Fluctuations, Energy Spectra, and Vortical Regions in Superfluid Turbulence, Phys. Rev. Lett. **109**, 205304 (2012).
[46] M. T. Reeves, B. P. Anderson, and A. S. Bradley, Classical and quantum regimes of two-dimensional turbulence in trapped Bose-Einstein condensates, Phys. Rev. A **86**, 053621 (2012).
[47] A. W. Baggaley, C. F. Barenghi, and Y. A. Sergeev, Three-dimensional inverse energy transfer induced by vortex reconnection, Phys. Rev. E **89**, 013002 (2014).
[48] S. K. Nemirovskii, Reconnection of quantized vortex filaments and the Kolmogorov spectrum, Phys. Rev. B **90**, 104506 (2014).
[49] A. Villois, D. Proment, and G. Krstulovic, Evolution of a superfluid vortex filament tangle driven by the Gross-Pitaevskii equation, Phys. Rev. E **93**, 061103(R) (2016).
[50] T. Yasuda, S. Goto, and G. Kawahara, Quasi-cyclic evolution of turbulence driven by a steady force in a periodic cube, Fluid Dyn. Res. **46**, 061413 (2014).
[51] See Supplemental Material at http://link.aps.org/supplemental/10.1103/PhysRevFluids.3.104606 for movies of the dynamics.
[52] M. V. Melander and F. Hussain, Core dynamics on a vortex column, Fluid Dyn. Res. **13**, 1 (1994).
[53] R. M. Kerr, Vortex Stretching as a Mechanism of Quantum Kinetic Energy Decay, Phys. Rev. Lett. **106**, 224501 (2011).